Pergamon

Int. J. Heat Mass Transfer. Vol. 38, No. 13, pp. 2343–2352, 1995

0017–9310/95 $9.50+0.00

0017–9310(94)00359–9

Three-dimensional natural convection flow around two interacting isothermal cubes

DON J. CHA† and SOYOUNG S. CHA‡

Department of Mechanical Engineering, University of Illinois at Chicago, 2039 ERF, 842 W. Taylor St, Chicago, IL 60607, U.S.A.

(*Received* 18 *May* 1994 *and in final form* 1 *December* 1994)

Abstract—Laminar steady buoyancy-driven flow around two interacting isothermal cubes in an infinite medium is investigated by employing a control-volume finite difference technique and holographic interferometry. The two cubes are positioned along the diagonal direction. Parametric investigations are performed by varying the center-to-center cube spacing and by varying the Rayleigh number while the Prandtl number is kept constant. To validate the numerical solutions, the calculated isothermal contours are qualitatively compared with the isophase lines in pathlength-integrated holographic interferograms. The heat transfer results are presented in terms of the average Nusselt number and the face-average Nusselt numbers at individual walls of each cube.

INTRODUCTION

The study of natural convection around solid objects can be of great importance in many engineering applications. Especially for interacting bodies, the interest in obtaining their quantitative information has increased considerably, mainly due to the advances in solar heating technology, nuclear reactor safety, and waste disposal. The demands for cooling of electronic components and environmental thermal transport in large buildings have also increased its importance for better understanding of natural convection in interacting flow fields. There exists an abundance of examples for two-dimensional heat transfer, either experimental [1, 2] or numerical [3, 4]: however, it appears that the previously published results for interacting three-dimensional (3D) external natural convection flows are very scant. Even for single 3D objects, only a few works have been reported. Some typical examples are those by Sparrow and Ansari [5], Churchill [6], and Cha and Cha [7] for a short cylinder, a sphere and a cube, respectively. Sparrow and Stretton [8] experimentally studied natural convection from cubes oriented in various directions and formulated means for correlating the heat transfer phenomena of some typical three-dimensional bodies. Tolpadi and Kuehn [9] reported a numerical study based on a vorticity and vector potential approach for the heat transfer from a horizontal cylinder with transverse circular fins. An additional example can be that of Worthington *et al.* [10], which presented electrochemical mass transfer and observed flow patterns by using Schlieren photography for a variety of cuboid geometries.

As a continuation of a previous work [7], we present here the numerical and experimental investigation results of 3D natural convection flows around two interacting isothermal cubes. We believe that this study can provide valuable knowledge for the aforementioned engineering applications.

MATHEMATICAL AND NUMERICAL FORMULATION

The geometrical configuration of the natural convection problem under investigation is depicted in Fig. 1. As shown in the figure, two smooth cubes of constant temperature T_w are immersed in an ambient fluid of temperature T_∞ to produce a buoyancy-driven flow. The two cubes are positioned along the 45° diagonal direction. The domain of computation consisted of three outer solid walls, an inner symmetry plane, an inflow boundary plane at the bottom, and an outflow boundary plane at the top, respectively. Since the flow is symmetric with respect to the y–z plane, only a half of the flow domain needs to be considered. A region of recirculation might be formed in the flow field. Consequently, all the terms in the governing equations were retained in order to keep the equations in an elliptic form. In computation, the Rayleigh number was varied from 1.3×10^3 to 1.0×10^5 for a fixed Prandtl number of 8940 that corresponds to the value of glycerin at a mean temperature of 25°C. The flow was thus expected to be in a laminar flow regime. Additionally, the 3D flow was assumed to be steady and incompressible with constant properties except density. Only gravity was considered as an external force.

† D. J. Cha is currently at U.S. Department of Energy, Morgantown Energy Technology Center, P.O. Box 880, Morgantown, WV 26507, U.S.A., as a National Research Council Research Associate.

‡ Author to whom correspondence should be addressed.

NOMENCLATURE

A area
g acceleration due to gravity
H center-to-center cube spacing
L, M, N numbers of grid division in x, y and z-directions
n normal direction to a cube surface
Nu local Nusselt number
$\overline{Nu}$ average Nusselt number based on S
$\overline{Nu_f}$ face-average Nusselt number similar to $\overline{Nu}$
p dimensionless pressure
Pr Prandtl number, ν/α
R residual of the continuity equation defined in ref. [11]
Ra Rayleigh number based on S, $\beta g S^3(T_w - T_\infty)/(\alpha\nu)$
S side length of a cube
T fluid temperature
u, v, w dimensionless velocity components in the x, y and z-directions
x, y, z dimensionless coordinates
XL, YL, ZL dimensions of the computational domain in the x, y and z-directions.

Greek symbols
α thermal diffusivity
β volumetric coefficient of thermal expansion
$\delta x, \delta y, \delta z$ minimum grid spacings in x, y and z-directions
θ dimensionless temperature
ν kinematic viscosity
ρ density
ϕ dependent scalar variable.

Subscripts
w wall
∞ ambient fluid.

Superscripts
$'$ dimensional quantity.

The governing equations based on the aforementioned assumptions and associated boundary conditions were then nondimensionalized. The dimensionless governing equations thus formed with appropriate dimensionless variables are shown below.

$$x = x'/S \quad y = y'/S \quad z = z'/S$$
$$p = p'/(\rho(\alpha/S)^2) \quad u = u'/(\alpha/S)$$
$$v = v'/(\alpha/S) \quad w = w'/(\alpha/S)$$
$$\theta = (T - T_\infty)/(T_w - T_\infty). \tag{1}$$

Continuity equation:

$$\frac{\partial u}{\partial x} + \frac{\partial v}{\partial y} + \frac{\partial w}{\partial z} = 0. \tag{2}$$

x-momentum equation:

$$u\frac{\partial u}{\partial x} + v\frac{\partial u}{\partial y} + w\frac{\partial u}{\partial z} = Pr\left(\frac{\partial^2 u}{\partial x^2} + \frac{\partial^2 u}{\partial y^2} + \frac{\partial^2 u}{\partial z^2}\right) - \frac{\partial p}{\partial x}. \tag{3}$$

y-momentum equation:

$$u\frac{\partial v}{\partial x} + v\frac{\partial v}{\partial y} + w\frac{\partial v}{\partial z} = Pr\left(\frac{\partial^2 v}{\partial x^2} + \frac{\partial^2 v}{\partial y^2} + \frac{\partial^2 v}{\partial z^2}\right) - \frac{\partial p}{\partial y} + Ra\,Pr\,\theta. \tag{4}$$

z-momentum equation:

$$u\frac{\partial w}{\partial x} + v\frac{\partial w}{\partial y} + w\frac{\partial w}{\partial z} = Pr\left(\frac{\partial^2 w}{\partial x^2} + \frac{\partial^2 w}{\partial y^2} + \frac{\partial^2 w}{\partial z^2}\right) - \frac{\partial p}{\partial z}. \tag{5}$$

Energy equation:

$$u\frac{\partial \theta}{\partial x} + v\frac{\partial \theta}{\partial y} + w\frac{\partial \theta}{\partial z} = \frac{\partial^2 \theta}{\partial x^2} + \frac{\partial^2 \theta}{\partial y^2} + \frac{\partial^2 \theta}{\partial z^2}. \tag{6}$$

The Rayleigh number was defined by $Ra = \beta g S^3(T_w - T_\infty)/(\alpha\nu)$ as usual. The dimensionless boundary conditions associated with the governing equations are as follows.

Cubic source walls:

$$u = 0 \quad v = 0 \quad w = 0 \quad \theta = 1. \tag{7}$$

Outer solid walls:

$$u = 0 \quad v = 0 \quad w = 0 \quad \theta = 0. \tag{8}$$

y–z symmetry plane:

$$u = 0 \quad \frac{\partial v}{\partial x} = 0 \quad \frac{\partial w}{\partial x} = 0 \quad \frac{\partial \theta}{\partial x} = 0. \tag{9}$$

Inflow boundary plane:

$$u = 0 \quad \frac{\partial v}{\partial y} = 0 \quad w = 0 \quad \theta = 0. \tag{10}$$

Outflow boundary plane:

$$u = 0 \quad \frac{\partial v}{\partial y} = 0 \quad w = 0 \quad \frac{\partial \theta}{\partial y} = 0. \tag{11}$$

The governing equations and associated boundary conditions were discretized by a control-volume finite difference method. The SIMPLE algorithm [11] was employed. The convective and diffusive fluxes were

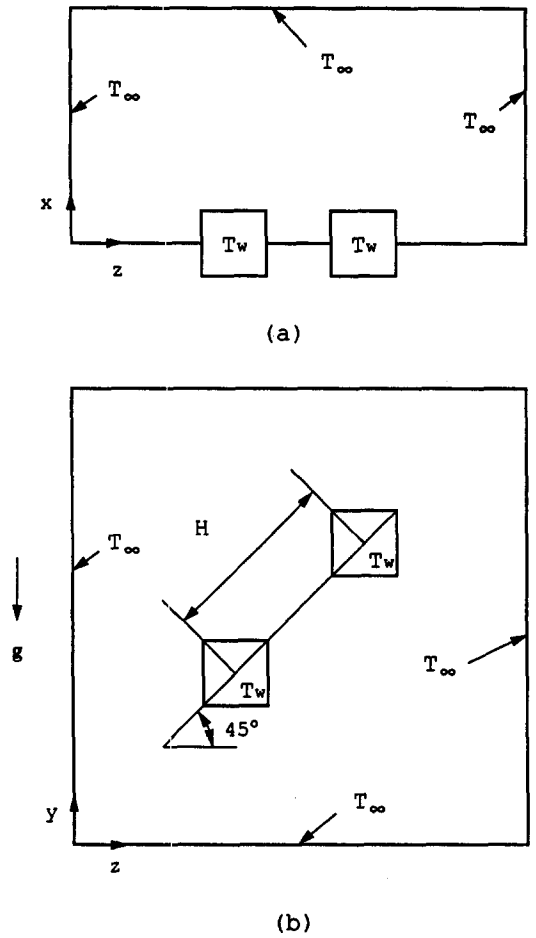

Fig. 1. Configuration of the natural convection field of investigation: (a) top view; (b) front view.

approximated by using the power law scheme [11, 12]. Some values required at the internal grid points located in the domain corresponding to two cubes, that is, $u = 0, v = 0, w = 0$ and $\theta = 1$, were maintained by manipulating the finite difference equations such that the source terms dominate all other terms [11]. The discretization equations were solved using a tri-diagonal matrix algorithm (TDMA) with a line-by-line method. Initially, the TDMA was applied to the grid lines in the x-direction, then by sweeping them along the y-and z-directions, respectively. Next, it was applied in the y-direction with the sweeping sequence of the z- and x-directions, respectively. Finally, it was applied in the z-direction in a similar manner. The direction of iteration was alternated such that the solution proceeded from one end to the other and vice versa. Underrelaxation [11] was employed to avoid divergence in the iterative solutions of these strongly nonlinear equations. The values of relaxation factors for the momentum and energy equations were varied from 0.1 to 0.4 and from 0.4 to 0.8, respectively. The convergence in the kth iteration tested with the following two criteria:

$$\left[1 - \frac{\phi^{k-1}}{\phi^k}\right]_{\max} < \varepsilon_1 \tag{12}$$

$$[|R|]_{\text{avg}} < \varepsilon_2. \tag{13}$$

where the symbols of ϕ and R denote the dependent scalar variable and residual defined in ref. [11]. The symbols of ε_1 and ε_2 are prescribed errors that were 2×10^{-4} and 1×10^{-5}, respectively, for the most of the runs in the current study.

Initially, rectangular pseudo outer boundaries on which flux boundary conditions could be applied, which might be better suited for this study, had been considered instead of the three outer solid walls. However, extensive numerical experiments showed that a rectangular pseudo boundary can cause premature instability [4] in computation, hindering the calculation of high Rayleigh number flows. Thus, the outer solid walls were assumed instead by choosing a domain that was determined such that further increase of its size would not affect much the numerical solution near the two cubes. This could be done by choosing the distances from five outermost faces of the two cubes to the corresponding facing walls of the domain to be approximately twice larger than the maximum thickness of the thermal boundary layers around a single cube. For validation, the boundary layer thicknesses around a single cube were found at several different Rayleigh numbers for sufficiently large flow domains with coarse nonuniform grids. Then, the approach for sizing the computational flow domain was applied to a single cube problem and the result was compared with that from holographic flow visualization [7]. This approach appears to be satisfactory. A nonuniform grid was used in all the x-, y- and z-directions. The neighborhood of the two cubes was more densely populated by grid-lines. Grid spacings, δx, δy and δz, were optimized by a trial-and-error procedure, but there were at least 10 nodes in a thermal boundary layer. More detailed discussions on both the computational domain size and grid spacing can be found in ref. [7].

The heat transfer around a cube can be presented in terms of the local Nusselt number, the face-average Nusselt number [13], and the average Nusselt number. The local Nusselt number at a cube surface is defined by

$$Nu = -\left.\frac{\partial\theta}{\partial n}\right|_{\text{w}} \tag{14}$$

where n is the direction normal to the cube surface. The local temperature gradient in Equation (14) was evaluated by using a three-point Taylor series expansion. The face-average Nusselt number $\overline{Nu}_{\text{f}}$ and the average Nusselt number $\overline{Nu}$ for a cube were determined by equations (15) and (16), respectively.

$$\overline{Nu}_{\text{f}} = -\int_{A_{\text{w}}} \left.\frac{\partial\theta}{\partial n}\right|_{\text{w}} \mathrm{d}A_{\text{w}} \tag{15}$$

Table 1. Input and output parameters for nonuniform grid calculation

Ra	$H/\sqrt{2}$	$\delta x \times \delta y \times \delta z$	$XL \times YL \times ZL$	$L \times M \times N$	No. of nodes
1.3×10^3	1.00	$0.05 \times 0.05 \times 0.05$	$1.7 \times 4.5 \times 4.4$	$25 \times 57 \times 58$	82650
1.3×10^3	1.25	$0.05 \times 0.05 \times 0.05$	$1.7 \times 4.8 \times 4.7$	$20 \times 52 \times 53$	55120
1.3×10^3	1.50	$0.05 \times 0.05 \times 0.05$	$1.7 \times 5.0 \times 4.9$	$20 \times 57 \times 58$	66120
1.3×10^3	1.75	$0.05 \times 0.05 \times 0.05$	$1.7 \times 5.3 \times 5.2$	$20 \times 62 \times 63$	78120
1.3×10^3	2.00	$0.05 \times 0.05 \times 0.05$	$1.7 \times 5.5 \times 5.4$	$20 \times 63 \times 64$	80640
1.0×10^4	1.25	$0.03 \times 0.03 \times 0.03$	$1.3 \times 4.8 \times 4.7$	$20 \times 67 \times 58$	71920
1.0×10^5	1.25	$0.02 \times 0.02 \times 0.02$	$1.0 \times 4.3 \times 3.3$	$19 \times 70 \times 60$	79800

$$\overline{Nu} = \frac{1}{6} \sum_{j=1}^{6} [\overline{Nu_f}]_j \tag{16}$$

where j denotes each surface of the cube. Here, only the face-average Nusselt number and the average Nusselt number are presented. However, all other involved quantities including the local Nusselt number were also calculated in the process of computation.

RESULTS AND DISCUSSION

The computer code used in this study had been verified by solving a three-dimensional natural convection flow around an isothermal cube [7]. Two parametric studies were performed by varying the center-to-center cube spacing H as shown in Fig. 1 and by varying the Rayleigh number. The geometry for a Rayleigh number of 1.3×10^3 was as follows. Initially, one cube was positioned at the other cube's upper right-hand corner: in other words, they were contacting each other along an edge and thus $H/\sqrt{2}$ was unity. The center of the upper cube was then moved along a 45° diagonal line. For other values of the Rayleigh number, only a fixed position was investigated. Typical parametric values employed for all the cases investigated are listed in Table 1. Figure 2 shows the holographic interferograms of the thermal plume from two isothermal cubes, captured at a specific projection angle perpendicular to the symmetry plane, at a Rayleigh number of 1.3×10^3 and $H/\sqrt{2}$ of 1.25. The details of the experiment are described in ref. [14]. Since the supporting bars of the cubes disturbed the adjacent flow field, two configurations were chosen, as shown in the figure, to produce a composite interferogram: one with the supporting bars on the right-hand side (RHS) and the other with them on the left-hand side (LHS), respectively. The complete projection interferogram was then obtained by combining those halves without the bars present. The interacting flow field of the two cubes can be clearly seen in Fig. 2. It was also found that the thermal boundary layers near the outermost faces of the cubes are thinner than the side length S of a cube. This holographic flow visualization could confirm that the computational domains determined according to the scheme explained before are sufficient not to affect the solutions near the two cubes.

Due to the similarity of the numerical solutions of all the cases involved, details of the results whose input parameters correspond to the flow visualization experiment shown in Fig. 2, that is, the case with Ra of 1.3×10^3 and $H/\sqrt{2}$ of 1.25, are only to be discussed. The isothermal contours and velocity vectors of this case are plotted in Fig. 3 for the vertical symmetric cross-section. Similar plots for velocity and temperature at a typical horizontal cross-section are also plotted in Fig. 4, however, showing only horizontal components for velocity. The shaded square areas in Figs. 3 and 4 represent both cubes and the upper one, respectively. Since the isothermal contour plots require interpolation of the data, i.e. B-cubic splines, the edges of the shaded areas were occasionally inconsistent with the nearest isothermal contour. However, this deficiency of the contour plots did not affect the evaluation of the local temperature gradients in equations (14)–(16), since only the original numerical results were used for this purpose. The isothermal contours in Fig. 3(a) were qualitatively compared with the interferometric fringes on the holographic interferograms in Fig. 2. The interferometric fringes approximately correspond to isophase lines, that is, equivalent contours of integrated optical pathlengths, of the three-dimensional flow field. As seen, the right half of Fig. 2(a) and the left half of Fig. 2(b) are in good agreement with their counterparts of Fig. 3(a). The temperature disturbance at the center symmetry plane is the dominating factor in integrating optical pathlengths, as evidenced in a previous investigation [7]. Consequently, even though the comparison is not direct, it can provide reasonable cross-comparison. A thorough quantitative comparison based on experimental tomographic reconstruction of the 3D field will follow in the future. As seen from both velocity vector plots in Figs. 3(b) and 4(b), rather strong flow entrainment from the surrounding toward the cubes was observed: however, no separation was observed at any corner of the cubes for the range of the Rayleigh numbers investigated. It was also observed that as the Rayleigh number increases, the thickness of the thermal boundary layer decreases.

Based on the argument that was presented in the previous study [7], it appears that the 3D numerical code works well and its numerical solutions are reliable. The average Nusselt numbers of both the upper and the lower cubes for Ra of 1.3×10^3 were calculated as a function of the center-to-center cube

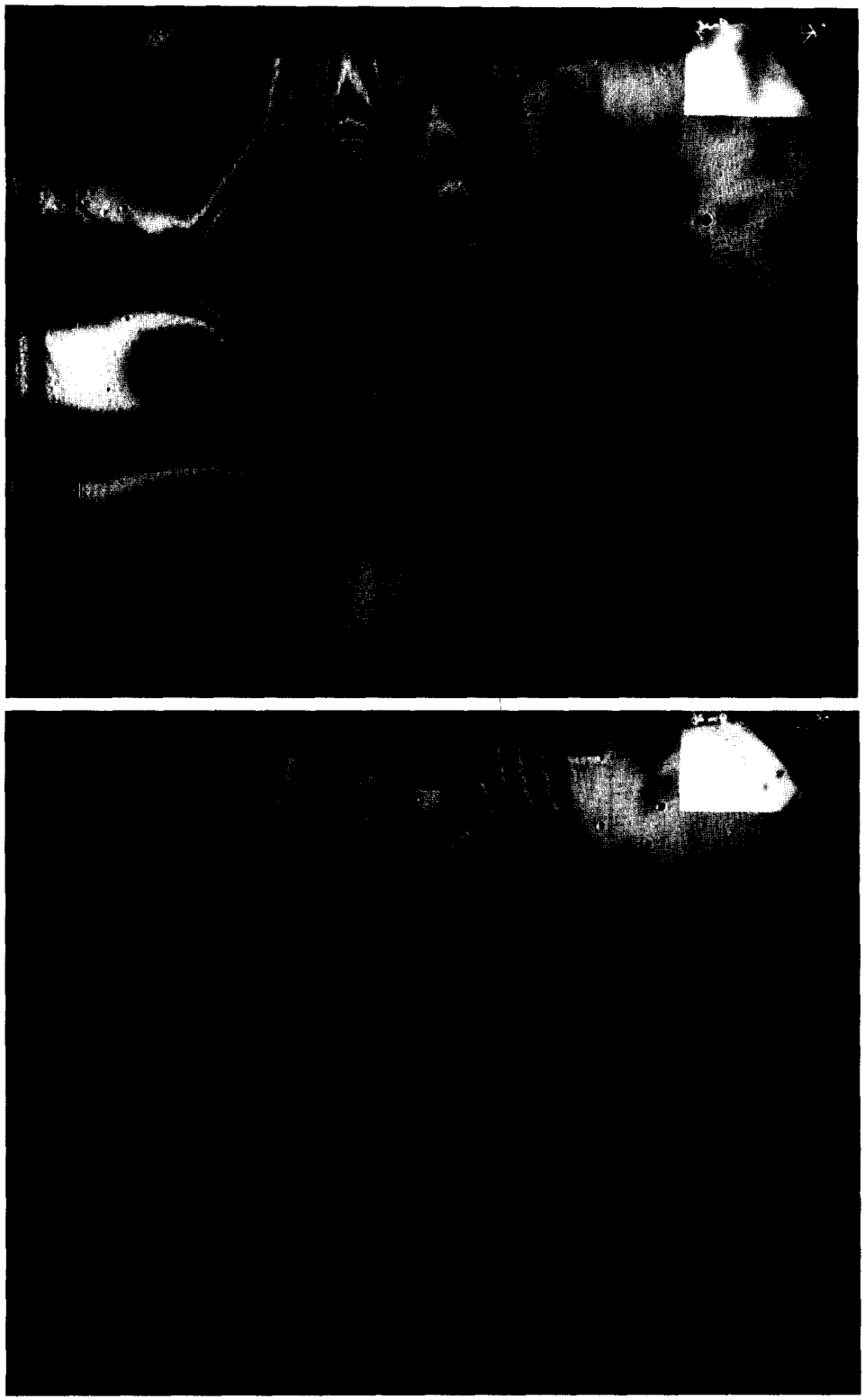

Fig. 2. Holographic interferograms of the thermal plume around two interacting cubes, projected normal to the symmetry plane: support legs at (a) RHS and (b) LHS.

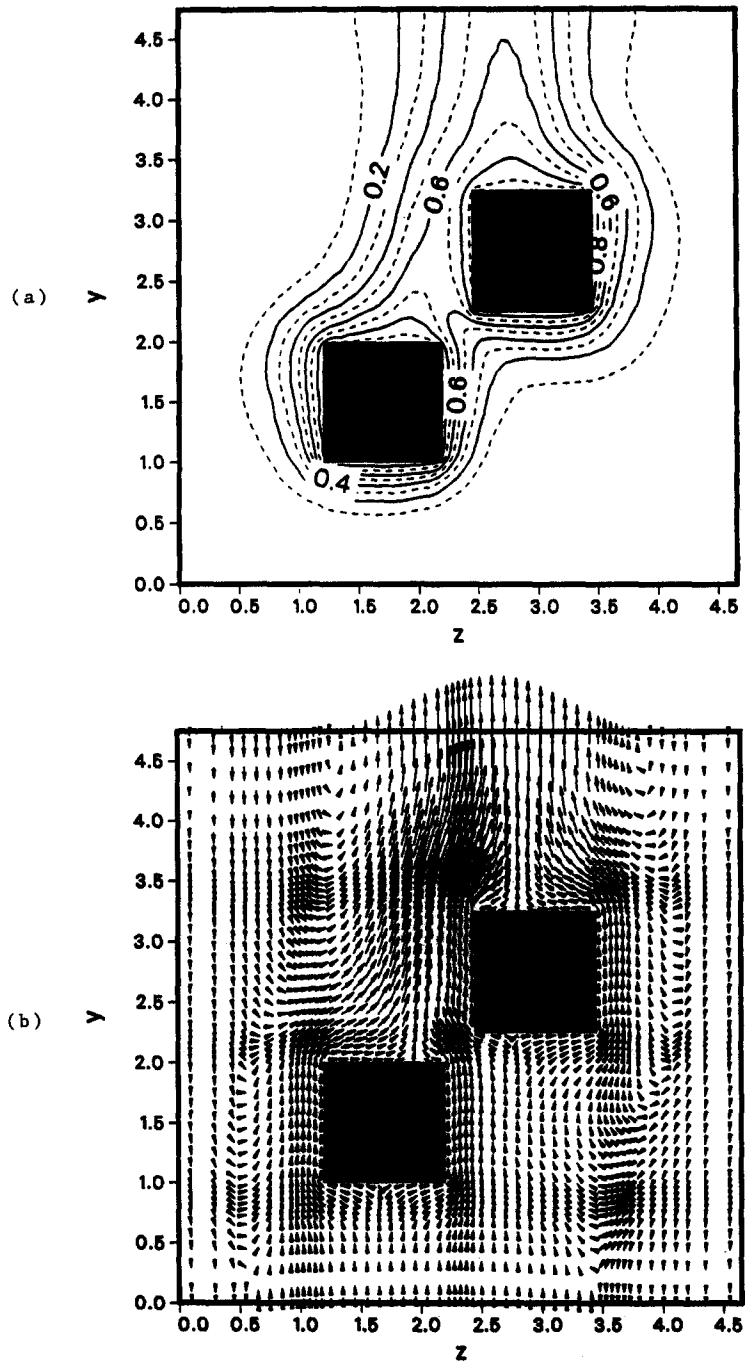

Fig. 3. Flow fields in the vertical symmetry plane for $Ra = 1.3 \times 10^3$ and $H/\sqrt{2} = 1.25$: (a) isothermal contours; (b) velocity vectors.

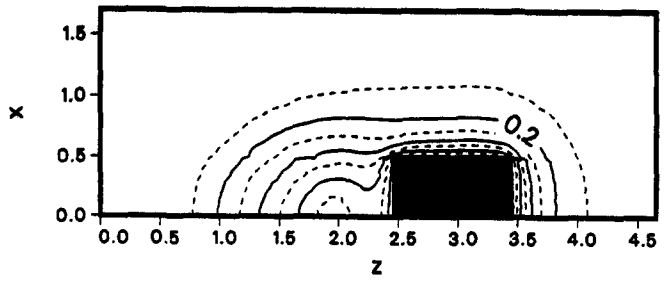

(a)

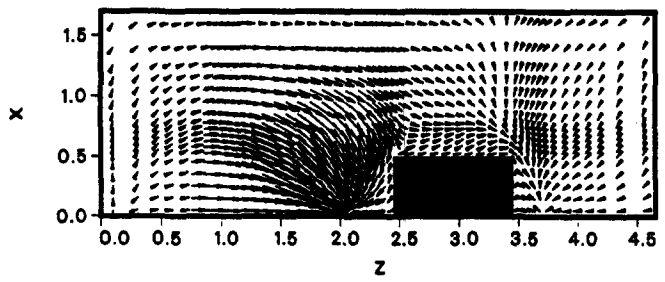

(b)

Fig. 4. Flow fields in the horizontal plane at a normalized distance of 0.05 from the upper cube bottom for $Ra = 1.3 \times 10^3$ and $H/\sqrt{2} = 1.25$: (a) isothermal contours; (b) horizontal velocity components.

spacing, and compared with that of a single cube [7]. Figure 5 shows these average values. When both cubes are in contact, the average Nusselt numbers of both of the cubes are minimum. The average Nusselt numbers of the lower cube are always larger than those of the upper cube but smaller than that of the single cube. For the range of the tested H-values as shown in Fig. 5, there still exists the effect of interacting thermal plumes, even though the average Nusselt numbers of both of the cubes gradually approach the single-cube value. However, it is believed that a substantial center-to-center cube spacing is required to reach the asymptotic single-cube value since the change beyond the maximum tested H-value is very gradual.

The face-average Nusselt numbers at the five different walls of each cube, that is, top, bottom, left, right, and back, were also calculated. The value at a front wall is the same as that at the corresponding back wall. Figures 6(a) and (b) show these five face-average Nusselt numbers of both the upper and the lower cube, respectively. The values for a single cube are also shown in Fig. 6 for cross-examination. That is, the face-average Nusselt numbers at the left, right, and back walls of both of the cubes can be compared with that at a vertical wall of the single cube and those at the top and bottom walls of the cubes directly with the corresponding values. As expected from the results of the average Nusselt numbers shown in Fig. 5, the face-average Nusselt numbers of the lower cube are in general larger than those of the upper cube. The face-average Nusselt numbers at the bottom, top, back, and left walls of the lower cube and at the bottom, back, and right walls of the upper cube are not affected much by the interaction of the flow fields as the center-to-center cube spacing varies except when $H/\sqrt{2}$ approaches the value of unity. Among these, for the changes near $H/\sqrt{2} = 1$, the bottom and top walls of the lower cube exhibit some significance while the bottom wall of the upper cube has greater variation.

The face-average Nusselt numbers at the right wall of the lower cube and at the left and the top wall of the upper cube change rather gradually over the cube spacing investigated. However, the former two show significant variation and they even exceed those corresponding single cube values as $H/\sqrt{2}$ becomes greater than about 1.5. The values at the bottom wall of the lower cube initially exceed the single cube counterpart but drop below as the cube spacing increases. All other face-average Nusselt numbers for the double cubes except for the aforementioned three

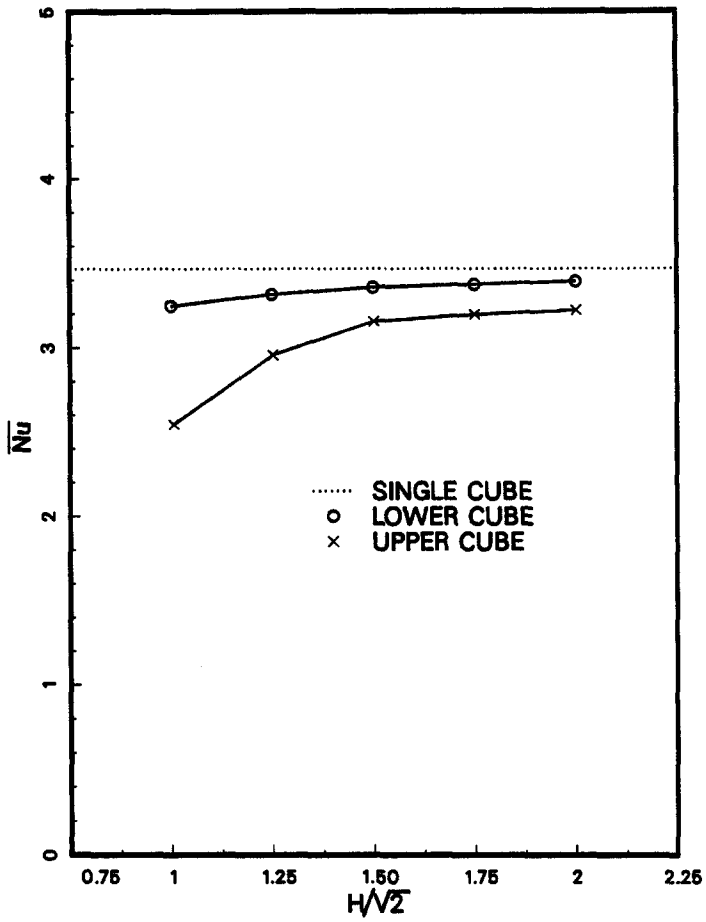

Fig. 5. Average Nusselt numbers of two interacting cubes for $Ra = 1.3 \times 10^3$ as a function of the center-to-center cube spacing.

are lower than the corresponding values for the single cube. It is believed that the asymptotic trend of the face-average Nusselt numbers, as previously discussed for the average Nusselt numbers, would also have been shown if the spacing had been extended further. The average Nusselt numbers of both the upper and lower cubes were calculated for the center-to-center cube spacing at $H/\sqrt{2} = 1.25$ as a function of the Rayleigh number and compared with those of the single cube as shown in Fig. 7. Similar to the results shown in Fig. 5, the average Nusselt numbers of the lower cube are larger than those of the upper cube but smaller than that of the single cube for the range of Rayleigh numbers investigated.

CONCLUSION

A 3D natural convection problem has been discussed, which can be produced around two interacting isothermal cubes in an infinite medium, at a high Prandtl number. Numerical solutions were obtained for a wide range of both Rayleigh numbers and the center-to-center cube spacings. In order to validate the numerical method, the calculated isothermal contours were qualitatively compared with the isophase lines in holographic interferograms. These comparisons were reasonably in good agreement. The heat transfer results were presented in terms of the average Nusselt number and the face-average Nusselt numbers at the top, bottom, left, right and back walls of the two cubes. This study may provide some valuable information for better understanding the 3D natural convection of interacting plume flow fields.

Acknowledgement—The authors gratefully acknowledge the support for this research in part by the National Science Foundation.

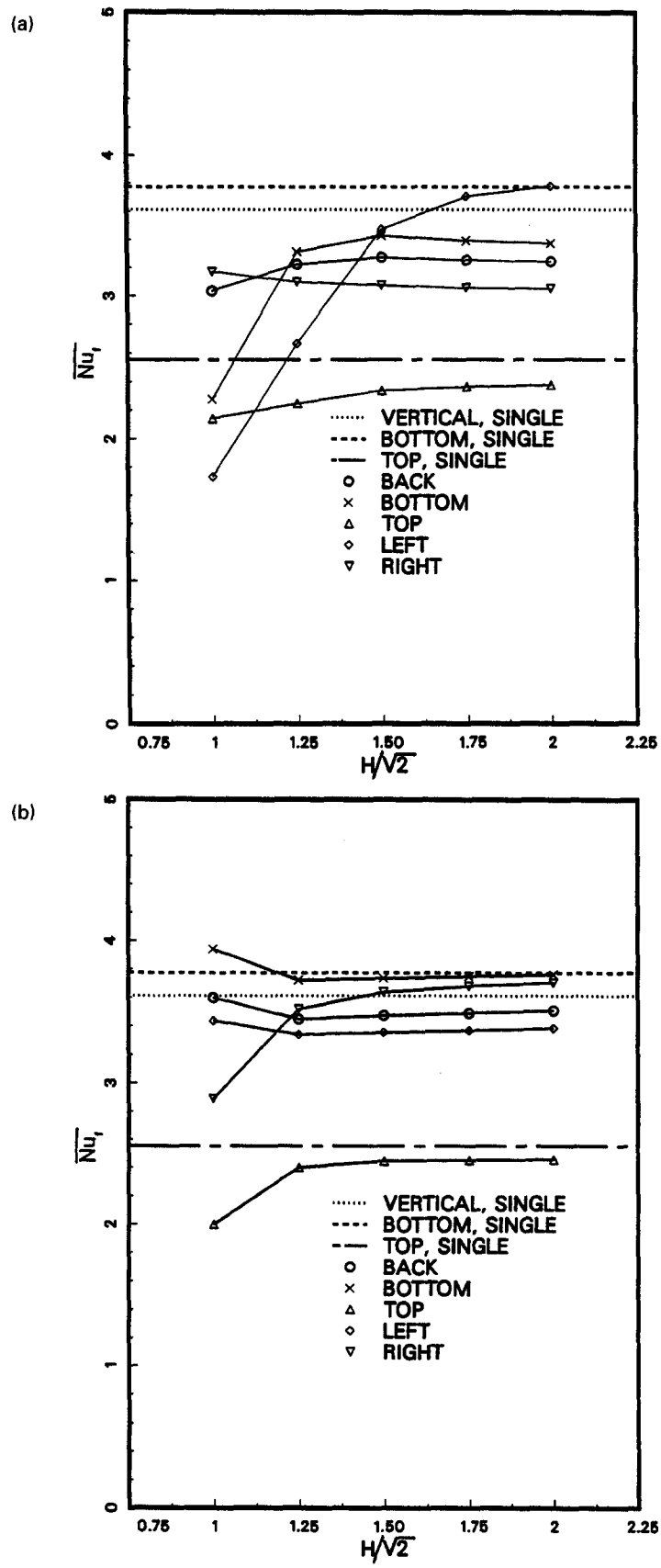

Fig. 6. Face-average Nusselt numbers at the five different walls of both (a) the upper and (b) the lower cube as a function of the center-to-center cube spacing.

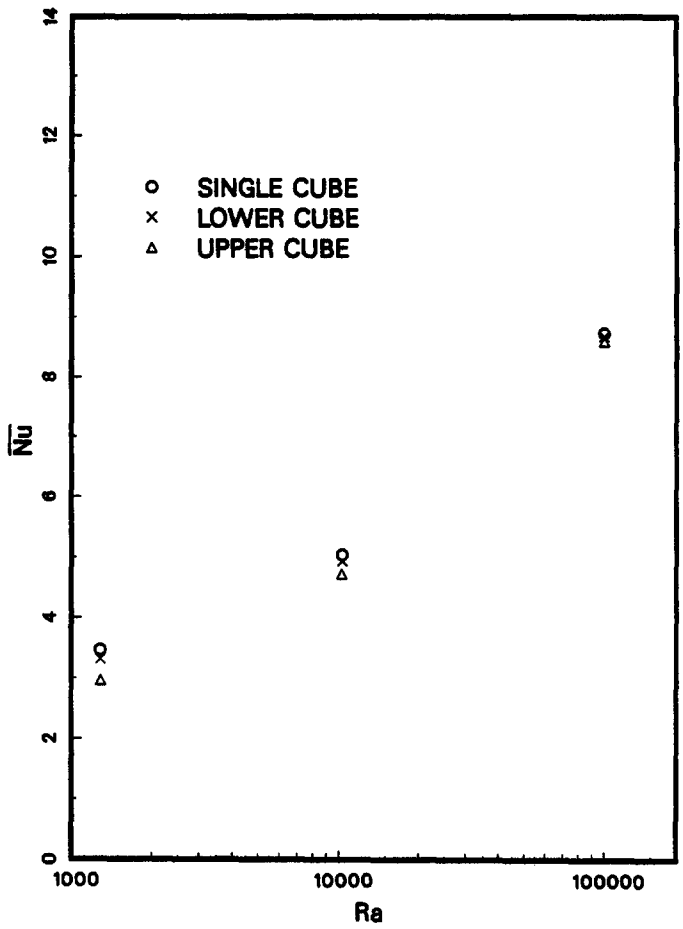

Fig. 7. Average Nusselt numbers of two interacting cubes for $H/\sqrt{2} = 1.25$ as a function of Rayleigh number.

REFERENCES

1. E. R. G. Eckert and E. Soehngen, Studies on heat transfer in laminar free convection with Zehnder-Mach interferometer, USAF Technical Report 5745 (1948).
2. B. Gebhart, H. Shaukatullah and L. Pera, The interaction of unequal laminar plane plumes, *Int. J. Heat Mass Transfer* **19,** 751–756 (1976).
3. B. Farouk and S. I. Guceri, Natural convection from horizontal cylinders in interacting flow fields, *Int. J. Heat Mass Transfer* **26,** 231–243 (1983).
4. S. Park and K. Chang, Pattern of interactive natural convection from two horizontal square cylinders, *Int. Commun. Heat Mass Transfer* **14,** 429–436 (1987).
5. E. M. Sparrow and M. A. Ansari, A refutation of King's rule for multi-directional experimental natural convection, *Int. J. Heat Mass Transfer* **26,** 1357–1363 (1983).
6. S. W. Churchill, Comprehensive, theoretically based, correlating equations for free convection from isothermal spheres, *Chem. Engng Commun.* **24,** 339–352 (1983).
7. D. J. Cha and S. S. Cha, Three-dimensional natural convection flow around an isothermal cube, *Int. Commun. Heat Mass Transfer* **20,** 619–630 (1993).
8. E. M. Sparrow and A. J. Stretton, Natural convection from variously oriented cubes and from other bodies of unity aspect ratio, *Int. J. Heat Mass Transfer* **28,** 741–752 (1985).
9. A. K. Tolpadi and T. H. Kuehn, Numerical study of three-dimensional natural convection from a horizontal cylinder with transverse circular fins, *Proceedings of the Eighth International Heat Transfer Conference*, Vol. 3, pp. 1305–1310 (1986).
10. D. H. Worthington, M. A. Patrick, and A. A. Wragg, Effect of shape on natural convection heat and mass transfer at horizontally oriented cubroids, *Chem. Engng Res. Des.* **65,** 131–138 (1987).
11. S. V. Patankar, *Numerical Heat Transfer and Fluid Flow.* Hemisphere, New York (1980).
12. S. V. Patankar, Elliptic systems: finite-difference method—I. In *Handbook of Numerical Heat Transfer* (Edited by W. J. Minkowycz, E. M. Sparrow, G. E. Schneider and R. H. Pletcher), Chap. 6. Wiley, New York (1988).
13. I. Olsen, B. W. Webb, and M. Queiroz, Local three-dimensional convective heat transfer from a heated cube, *ASME Heat Transfer Div. Publ. HTD* **123,** 7–13 (1989).
14. D. J. Cha, Interferometric tomography: reconstruction algorithm, experiment and comparison with a numerical study, Ph.D. Thesis, University of Illinois, Chicago, Illinois (1993).